
SPARSE LINEAR NETWORKS WITH A FIXED BUTTERFLY STRUCTURE: THEORY AND PRACTICE

Nir Ailon

Faculty of Computer Science
Technion Israel Institute of Technology
Haifa, Israel
nailon@cs.technion.ac.il

Omer Leibovich

Faculty of Computer Science
Technion Israel Institute of Technology
Haifa, Israel
leibovich@campus.technion.ac.il

Vineet Nair

Faculty of Computer Science
Technion Israel Institute of Technology
Haifa, Israel
vineet@cs.technion.ac.il

March 14, 2022

ABSTRACT

Fast Fourier transform, Wavelets, and other well-known transforms used in signal processing have a structured representation as a product of sparse matrices. Such representations are referred to as butterfly structures. Extensive research in the recent past have used such structured linear networks coupled with randomness as pre-conditioners to improve the computational performance of large scale linear algebraic operations. With the advent of deep learning and AI and given the computational efficiency of such structured matrices, it is natural to study sparse linear deep networks in which the location of the non-zero weights are predetermined by the butterfly structure. This work studies, both theoretically and empirically, the feasibility of training such networks in different scenarios.

Unlike convolutional neural networks (CNN's), which are structured sparse networks designed to recognize local patterns in lattices representing a spatial or a temporal structure, the butterfly architecture used in this work can replace *any* dense linear operator with a gadget consisting of a sequence of logarithmically (in the network width) many sparse layers, containing a total of near linear number of weights. This improves on the quadratic number of weights required in a standard dense layer, with little compromise in expressibility of the resulting operator.

We show in a collection of empirical experiments that our proposed architecture not only produces results that match and often outperform existing known architectures, but it also offers faster training and (as expected by the reduction in number of weights) prediction in deployment. This empirical phenomenon is observed in a wide variety of experiments that we report, including both supervised prediction on NLP and vision data, as well as in unsupervised representation learning using autoencoders. Preliminary theoretical results presented in the paper explain why training speed and outcome are not compromised by our proposed approach.

1 Introduction

A Butterfly network (see Figure 1) is a layered graph connecting a layer of n inputs to a layer of n outputs with $O(\log n)$ layers, where each layer contains $2n$ edges. The edges connecting adjacent layer are organized in disjoint gadgets, each gadget connecting a pair of nodes in one layer with a corresponding pair in the next layer by a complete graph. The distance between pairs doubles from layer to layer. This network structure represents the execution graph of the FFT (Fast Fourier Transform) [CT65], Walsh-Hadamard transform, and many important transforms in signal processing that are known to have fast algorithms to compute matrix-vector products.

In 2006, Ailon and Chazelle [AC09] showed how to use the Fourier (or Hadamard) transform to perform fast Euclidean dimensionality reduction with Johnson-Lindenstrauss guarantees [JL84]. The resulting transformation, called Fast Johnson-Lindenstrauss Transform (FJLT), was improved in subsequent works [AL09, KW11]. The common theme in this line of work is in defining fast randomized linear transformations that are composed of a random diagonal matrix, followed by a dense orthogonal transformation with a butterfly computational structure, followed by a projection onto a subset of coordinates. (In fact, this research is still active, see e.g.[JPS20]). FJLT (random) matrices are used as

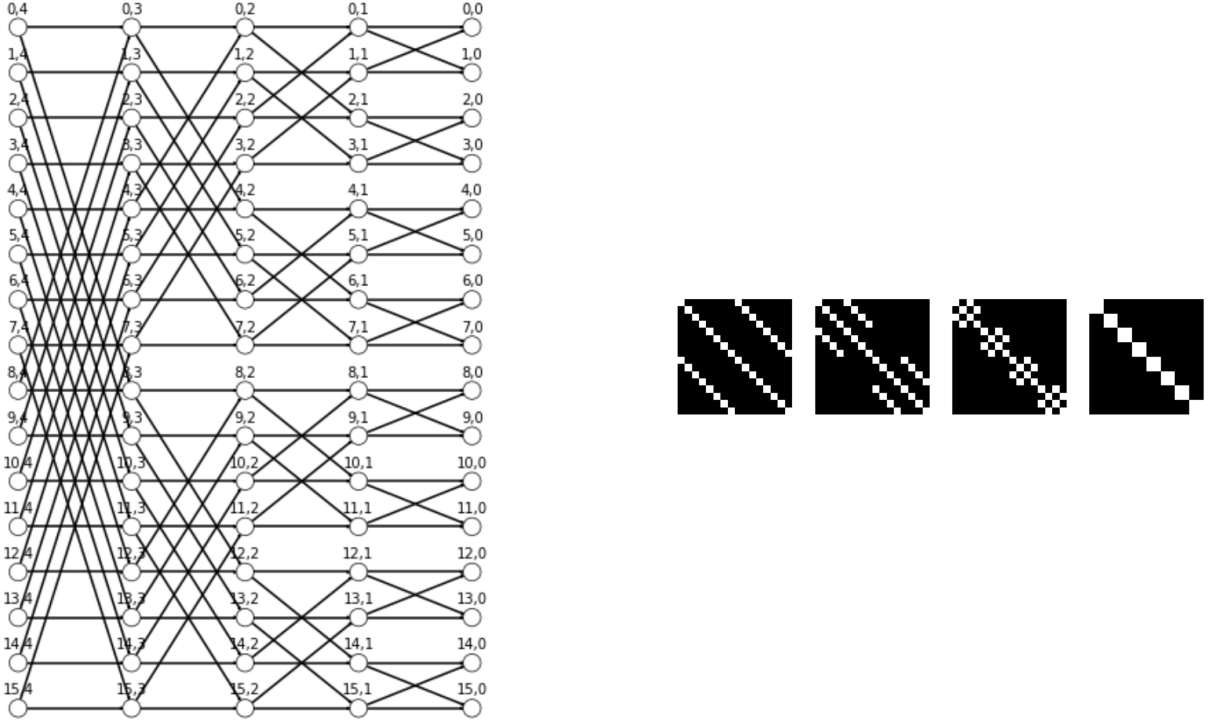


Figure 1: A 16×16 butterfly gadget represented as a 4-layered graph on the left, and as product of 4 sparse matrices on the right. The white entries are the non-zero entries of the matrices.

dimensionality reduction matrices, which allow computation of large scale linear algebra in lower dimensional space with little compromise of accuracy [Sar06, AM10]. This is achieved using a property known as *subspace embedding*. It is natural to ask whether FJLT-like transformations, implemented using butterfly architectures can be used to reduce dimensionality of wide, dense linear layers (see Section 4.1 for a detailed description of this idea). The clear advantages of such a strategy are (1) that almost all choices of weights from a specific distribution, namely the one mimicking FJLT, preserve accuracy while reducing dimensionality, and (2) the number of weights is near linear in the layer width. The drawbacks are that (1) the butterfly structure adds logarithmic depth to the architecture and (2) the sparse structure of the matrices connecting these layers defies the general theoretical analysis of convergence of deep linear networks. Our preliminary work provides both theoretical and empirical evidence that the advantages outweigh the drawbacks. We base our results both on prediction tasks, and on representation learning tasks using deep linear encoder-decoder architectures.

Note: One could argue that CNN’s (convolutional neural networks) already use a similar structure. But CNN’s are applied to layers that have a grid-like temporal or spatial structure, whereas randomized butterfly shaped preconditioners, such as FJLT, work with coordinate systems that are organized in any way.

2 Our Contribution

We provide an empirical report, together with a theoretical analysis.

On the empirical side – we report the outcomes of the following experiments:

(1) Replacing dense linear layers in the standard state-of-the-art networks, for both image and language data, with a composition of (a) a truncated butterfly network, (b) a dense linear layer in low dimension, and (c) a transposed truncated butterfly network. The structure parameters are chosen so as to keep the number of weights near linear (instead of quadratic).

(2) Training linear encoder-decoder networks, in which the encoder is either a truncated butterfly network, or a composition of a truncated butterfly network and a dense linear transformation. In either case, the network structure parameters are chosen so as to keep the number of weights in the encoder near linear in the input dimension. Our results

demonstrate that this has little to no effect on the performance, compared to dense linear encoder-decoder networks (i.e. PCA).

(3) Inspired by the recent work of Indyk et al [IVY19] we show how to learn to perform low-rank matrix approximation, given a sample of matrices and a fixed butterfly based network architecture.

We note that, as far as we know, this is the first reported attempt to train butterfly shaped networks in which the weights on the butterfly network are trained (and not fixed in advanced).

On the theoretical side – The optimization landscape of linear neural networks with dense matrices have been studied by Baldi and Hornik [BH89], and Kawaguchi [Kaw16]. The theoretical part of this work studies the optimization landscape of the encoder-decoder network with a butterfly gadget: a three layer linear neural network where the first layer is a truncated butterfly gadget and the remaining two layers are dense. Let $X \in \mathbb{R}^{n \times d}$ and $Y \in \mathbb{R}^{m \times d}$ be the data and output matrices respectively. Then the *encoder-decoder butterfly network* is given as $\bar{Y} = DEBX$, where $D \in \mathbb{R}^{m \times k}$ and $E \in \mathbb{R}^{k \times \ell}$ are dense layers, and B is the $\ell \times n$ truncated butterfly gadget (product of $\log n$ sparse matrices) and $k \leq \ell \leq m \leq n$ (see Section 4.2). The objective is to learn D, E and B that minimizes $\|\bar{Y} - Y\|_F^2$. Theorem 1 shows how the loss at the critical points of such a network depends on the eigenvalues of the matrix $\Sigma = YX^T B^T (BXX^T B^T)^{-1} BXY^T$ ¹. In comparison, the loss at the critical points of an encoder-decoder network (without the butterfly gadget) depends on the eigenvalues of the matrix $\Sigma' = YX^T (XX^T)^{-1} XY^T$ [BH89]. In particular, Theorem 1 shows that the loss depends on how the learned matrix B changes the eigenvalues of Σ' . If we learn only for an optimal D and E , keeping B fixed then Theorem 1 shows in this case every local minima is a global minima and the loss at the local/global minima depends on how B changes the top k eigenvalues of Σ' . This and [Sar06] together give worst-case guarantee in the special case when $Y = X$ (called auto-encoders) (see the third remark after Theorem 1).

3 Related Work

Important transforms like discrete Fourier, discrete cosine, Hadamard and many more satisfy a property called *complementary low-rank* property, recently defined in [LYM⁺15]. For an $n \times n$ matrix satisfying this property related to approximation of specific submatrices by low-rank matrices, Michielssen and Boag, and Niel et al. [MB96, OWR10] developed the butterfly algorithm to compute the product of such a matrix with a vector in $O(n \log n)$ time. In general, the butterfly algorithm has a pre-computation stage which requires $O(n^2)$ time [OWR10, Sel12], but for many transforms as given in [CDY09, LYY15, PDMY14, Yin09, DY12] this pre-computation cost is linear. The butterfly algorithm factorizes such a matrix into $O(\log n)$ many matrices, each with $O(n)$ sparsity. With the objective of reducing the pre-computation cost Li et al. [LYM⁺15, LY17] compute the butterfly factorization for an $n \times n$ matrix satisfying the complementary low-rank property in $O(n^{\frac{3}{2}})$ time. This line of work does not learn butterfly representations for matrices or apply it in neural networks, and is incomparable to our work.

Dao et al. [DGE⁺19] show how one can learn a butterfly structure of standard transformations, given examples. Their work defers from ours, because we assume that the butterfly structure is known with respect to a fixed (yet arbitrary) choice of coordinate system, and we allow changing the weights on the corresponding butterfly edges.

A few works in the past have used deep learning models with structured matrices (as hidden layers). Such structured matrices can be described using fewer parameters compared to a dense matrix, and hence a representation can be learned by optimizing over a fewer number of parameters. Examples of structured matrices used include low-rank matrices [DSD⁺13, SKS⁺13], circulant matrices [CYF⁺15, DLW⁺17], low-distortion projections [YMD⁺15], Toeplitz like matrices [SSK15, LSS16, YWL⁺18], Fourier-related transforms [MDAdF16] and matrices with low-displacement rank [TGD⁺18]. These models were primarily considered for applications to resource-constraint environment, and although these models provide computational benefits, they generally are not better than dense (unstructured) matrices. The closest to our work are [YMD⁺15] and [MDAdF16]. They attempt to replace dense, linear layers with a stack of structured matrices, including a butterfly structure (the Hadamard or the Cosine transform), but they do not place trainable weights on the edges of the butterfly structure as we do. Note that adding these trainable weights does not compromise the run time benefits in prediction, while adding to the expressiveness of the network.

Finally, we mention the work of Indyk et al [IVY19], who study whether it is possible to learn, given a sample of matrices, a unique subspace embedding transformation for these matrices, where the transformation belongs to the family of sparse matrices as defined in Clarkson et al's highly influential work [CW09] on fast low rank matrix approximation. As in our work, they place trainable weights on the transformation's non-zero locations. We dedicate a section of experiments to apply our butterfly architecture with their setting.

¹At a critical point the gradient of the loss function with respect to the parameters in the network is zero.

4 Preliminaries and Notation

All logarithms are in base 2. $[n]$ denotes the set $\{1, \dots, n\}$.

Definition 4.1 (Butterfly Gadget). *Let n be an integral power of 2. Then an $n \times n$ butterfly gadget B (see Figure 1) is a stack of $\log n$ linear layers, where in each layer $i \in \{0, \dots, \log n - 1\}$, a bipartite clique connects between pairs of nodes $j_1, j_2 \in [n]$, for which the binary representation of $j_1 - 1$ and $j_2 - 1$ differs only in the i 'th bit. In particular, the number of edges in each layer is $2n$.*

We will denote the matrix corresponding to the action of the i 'th layer in a butterfly gadget by W_i . In what follows, a *truncated butterfly gadget* is a butterfly gadget in which the deepest layer is truncated, namely, only a subset of ℓ neurons are kept and the remaining $n - \ell$ are discarded. The integer ℓ is a tunable parameter, and the choice of neurons is always assumed to be sampled uniformly at random and fixed throughout training in what follows.

The effective number of parameters (trainable weights) in a truncated butterfly gadget is equal to $O(n \log \ell)$, for any ℓ and any choice of neurons (for a proof of this combinatorial fact, see [AL09]).

The reason for studying a truncated butterfly gadget follows (for example) from the work [AC09, AL09, KW11]. These papers define randomized linear transformations with the Johnson-Lindenstrauss property and an efficient computational graph which essentially defines the truncated butterfly gadget. In what follows, we will collectively denote these constructions by FJLT (Fast Johnson-Lindenstrauss Transforms).²

For $X \in \mathbb{R}^{n \times d}$ the best rank k approximation of X is denoted X_k , and $\|X_k - X\|_F^2 = \Delta_k$. Sarlos [Sar06] proved that with high probability a good low-rank approximation of X can be computed even when X is pre-processed with an FJLT to reduce the dimension. In particular with probability at least $1/2$, the best rank k approximation of X from the rows of JX (denoted $J_k(X)$), where J is sampled from an $\ell \times n$ FJLT distribution and $\ell = (k \log k + k/\epsilon)$ satisfies $\|J_k(X) - X\|_F^2 \leq (1 + \epsilon)\Delta_k$. Thus such a pre-processing matrix improves the computational and memory requirements of low-rank approximation without much loss in accuracy. In their seminal work in [CW09], Clarkson and Woodruff showed that good approximation could also be obtained when J is sampled as an $\ell \times n$ sparse random sketching matrix with one non-zero entry in each column – the non-zero location for each column are chosen uniformly at random and the non-zero entries are set to $+1$ or -1 uniformly at random. Clarkson and Woodruff proved that if $\ell = k \log(1/\delta)/\epsilon$, $\epsilon > 0$, $0 < \delta < 1$ and J is sampled as an $\ell \times n$ sparse sketching matrix then with probability at least $(1 - \delta)$, $\|J_k(X) - X\|_F^2 \leq (1 + \epsilon)\Delta_k$.

4.1 Matrix Approximation Using Butterfly Networks

Suppose $J_1 \in \mathbb{R}^{k_1 \times n_1}$ and $J_2 \in \mathbb{R}^{k_2 \times n_2}$ are matrices sampled from FJLT distribution, and let $W \in \mathbb{R}^{n_2 \times n_1}$. Then using standard JL arguments it follows that for the random matrix $W' = J_2^T J_2 W J_1^T J_1$, and any unit vector $u \in \mathbb{R}^{n_1}$ and any $\epsilon \in (0, 1)$,

$$\Pr[\|W'u - Wu\| \leq \epsilon \|W\|] \geq 1 - e^{-\Omega(\min\{k_1, k_2\}\epsilon^2)}.$$

Hence, W' approximates the action of W with high probability on any given input vector. Now notice that W' can be written as $J_2^T \tilde{W} J_1$ where J_1 (resp. J_2^T) are expressible as a truncated butterfly gadget (resp. transposed butterfly gadget), and \tilde{W} is a $k_1 \times k_2$ (dense) matrix. Therefore, in a deep network, we should generally be able to replace a dense linear layer connecting n_1 neurons to n_2 neurons (containing $n_1 n_2$ variables) with a composition of three gadgets, where two have a butterfly shape and contain near linearly many weights, and one is dense with $k_1 k_2$ variables. We experiment with this idea in Section 5.1, where the butterfly gadgets are initialized by sampling it from an FJLT distribution, and the dense matrices are initialized randomly as in Pytorch.

4.2 Encoder-Decoder Network with a Butterfly Gadget

Let $X \in \mathbb{R}^{n \times d}$, and $Y \in \mathbb{R}^{m \times d}$ be data and output matrices respectively, and $k \leq m \leq n$. Then the encoder-decoder network for X is given as

$$\bar{Y} = DEX$$

where $E \in \mathbb{R}^{k \times n}$, and $D \in \mathbb{R}^{m \times k}$ are called the encoder and decoder matrices respectively. For the special case when $Y = X$, the encoder-decoder network is referred to as auto-encoders. The optimization problem is to learn matrices D and E such that $\|Y - \bar{Y}\|_F^2$ is minimized. The optimal solution is denoted as Y^* , D^* and E^* ³. In the case

²To be precise, the construction in [AC09, AL09, KW11] also uses a random diagonal matrix, but the values of the diagonal entries can be ‘swallowed’ inside the weights of the first layer of the butterfly gadget.

³Possibly multiple D^* and E^* exist such that $Y^* = D^* E^* X$.

Dataset Name	Task	Model
Cifar-10 [Kri09]	Image classification	EfficientNet [Kua]
Cifar-10 [Kri09]	Image classification	PreActResNet18 [Kua]
Cifar-100 [Kri09]	Image classification	seresnet152 [Wei]
Imagenet [DDS ⁺ 09]	Image classification	senet154 [Cad18]
CoNLL-03 [TKSDM03]	Named Entity Recognition (English)	Flair's Sequence Tagger [ABV18] [ABV19]
CoNLL-03 [TKSDM03]	Named Entity Recognition (German)	Flair's Sequence Tagger [ABV18] [ABV19]
Penn Treebank (English) [MSM93]	Part-of-Speech Tagging	Flair's Sequence Tagger [ABV18] [ABV19]

Table 1: Data and the corresponding architectures used in the fast matrix multiplication using butterfly matrices experiments.

of auto-encoders $X^* = X_k$. The encoder-decoder network composed with a butterfly gadget as shown below is studied in this work

$$\bar{Y} = DEBX. \quad (1)$$

Here, X , Y and D are as in the encoder-decoder network, $E \in \mathbb{R}^{k \times \ell}$ is a dense matrix, and B is an $\ell \times n$ truncated butterfly gadget. In the encoder-decoder network with a butterfly gadget the encoding is done using EB , and decoding is done using D . This reduces the number of parameters in the encoding matrix from kn as in the encoder-decoder network to $k\ell + O(n \log \ell)$. Again the objective is to learn matrices D and E , and the truncated butterfly gadget B such that $\|Y - \bar{Y}\|_F^2$ is minimized. The optimal solution is denoted as Y^* , D^* , E^* , and B^* . The problem of learning matrices D and E that minimize $\|Y - \bar{Y}\|_F^2$ for a fixed B is also considered, in which case the optimal solution is denoted as $B_k(Y)$, D_B , and E_B . Observe that for autoencoders $B_k(X)$ is the best rank k approximation of X computed from the rows of BX . If the truncated butterfly gadget B is sampled from the $\ell \times n$ FJLT distribution, where $\ell = k \log k + \frac{k}{\epsilon}$ and $\epsilon > 0$, then for such a B with probability at least $\frac{1}{2}$, $B_k(X) \leq (1 + \epsilon)\Delta_k$ [Sar06]. Experiments in Sections 5.2 and 5.3 train an encoder-decoder network with a butterfly gadget, where the butterfly gadget is initialized by sampling it from an FJLT distribution, and D and E are initialized randomly as in Pytorch.

5 Experiments

In this section we report the results of our experiments. For relevant notations and preliminaries refer Section 4.

5.1 Replacing Dense Linear Layers by Butterfly Gadgets

This experiment replaces a dense linear layer in common deep learning architectures with the network proposed in Section 4.1. The datasets and the corresponding architectures considered are summarized in Table 1. For each dataset and model, the objective function is the same as defined in the model, and the generalization and convergence speed between the original model and the modified one (called the butterfly model for convenience) are compared. Figures 2 and 3 depicts the test accuracy and $F1$ score of the original model and the butterfly model. Figure 4 shows that the test accuracy for the butterfly model trained with stochastic gradient descent is even better than the original model trained with Adam in the first few epochs, and Figure 5 shows a similar thing is true in NLP tasks. In almost all the cases the modified architecture does better than the normal architecture, both in the rate of convergence and in the final accuracy/ $F1$ score.

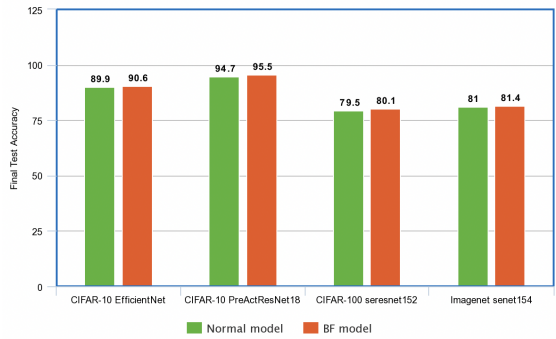


Figure 2: Final test accuracy comparison with different image classification models and data sets

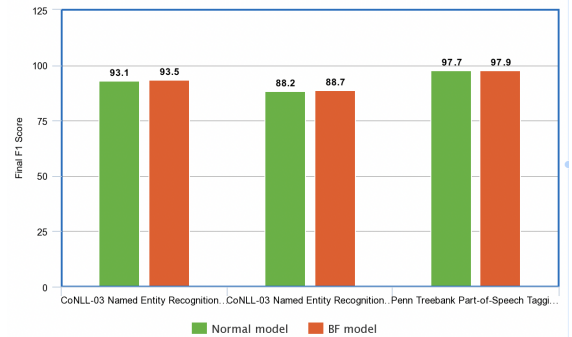


Figure 3: Final F1 Score for different NLP models and data sets

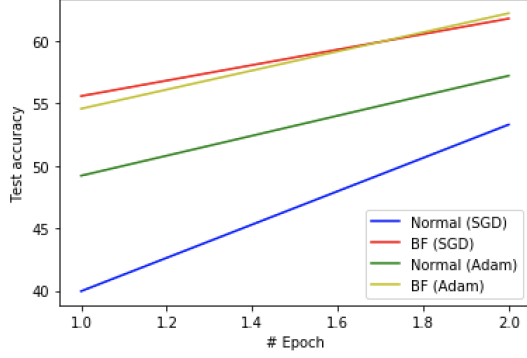


Figure 4: Test accuracy comparison with different models and optimizers on CIFAR-10 with PreArcResNet18.

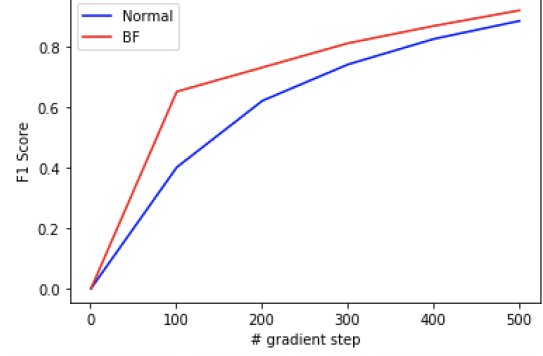


Figure 5: F1 comparison with different models on CoNLL-03 Named Entity Recognition (English) with the flair's Sequence Tagger

5.2 Truncated Butterfly Autoencoders on Synthetic Gaussian and Real Data

This experiment tests whether gradient descent based techniques can be used to train an auto-encoder with a truncated butterfly gadget (see Section 4.2). Five types of data matrices are tested: two are random and three are constructed using standard public real image datasets. For the matrices constructed from the image datasets, the input coordinates are randomly permuted, which ensures the network cannot take advantage of the spatial structure in the data.

Table 2 summarizes the data attributes. Gaussian 1 and Gaussian 2 are Gaussian matrices with rank 32 and 64 respectively. A Rank r Gaussian matrix is constructed as follows: r orthogonal vectors of size 1024 are sampled at random and the columns of the matrix are determined by taking random linear combinations of these vectors, where the coefficients are chosen independently and uniformly at random from the Gaussian distribution with mean 0 and variance 0.01. The data matrix for MNIST is constructed as follows: each row corresponds to an image represented as a 28×28 matrix (pixels) sampled uniformly at random from the MNIST database of handwritten digits [LC10] which is extended to a 32×32 matrix by padding numbers close to zero and then represented as a vector of size 1024 in column-first ordering⁴. Similar to the MNIST every row of the data matrix for Olivetti corresponds to an image represented as a 64×64 matrix sampled uniformly at random from the Olivetti faces data set [Cam94], which is represented as a vector of size 4096 in column-first ordering. Finally, for HS-SOD the data matrix is a 1024×768 matrix sampled uniformly at random from HS-SOD – a dataset for hyperspectral images from natural scenes [IOZ⁺18].

Name	n	d	rank
Gaussian 1	1024	1024	32
Gaussian 2	1024	1024	64
MNIST	1024	1024	1024
Olivetti	1024	4096	1024
HS-SOD	1024	768	768

Table 2: Data used in the truncated butterfly autoencoder reconstruction experiments.

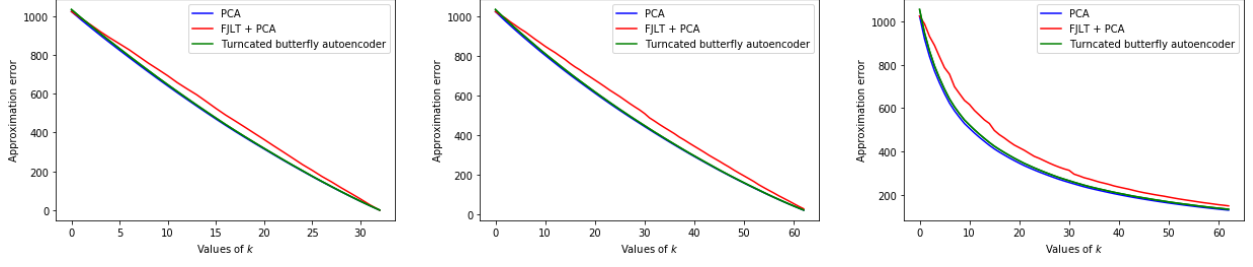
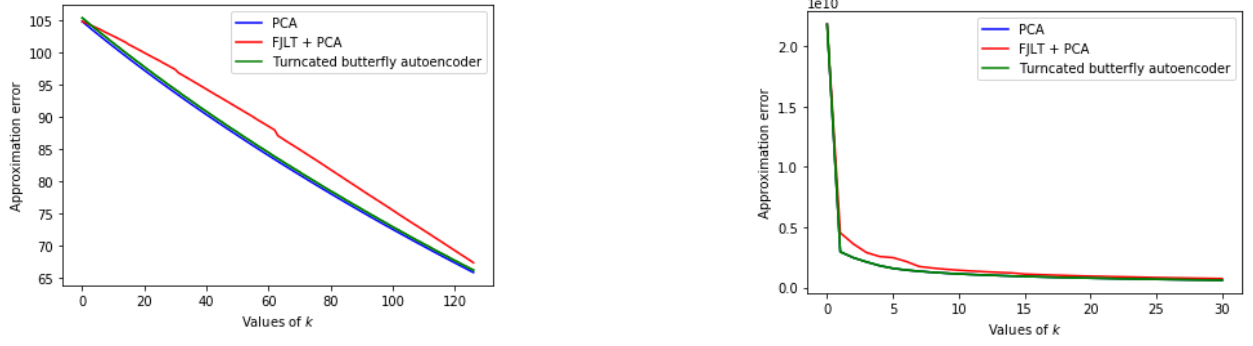
In Figures 6 and 7, for each of the above data matrices the loss obtained via training the truncated butterfly network with the Adam optimizer is compared to Δ_k (denoted as PCA) and $\|J_k(X) - X\|_F^2$ where J is an $\ell \times n$ matrix sampled from the FJLT distribution (denoted as FJLT+PCA)⁵. Note that for each of the above data matrices and for all values of k the loss for the encoder-decoder truncated butterfly network is almost equal to Δ_k , and is in fact Δ_k for small and large values of k .

5.3 Frozen Truncated Butterfly Followed by Dense Encoder-Decoder

This experiment is similar to the experiment in Section 5.2 but the training in this case is done in two phases. In the first phase, B is fixed and the network is trained to determine an optimal D and E . In the second phase, the optimal D and E determined in phase one are used as the initialization, and the network is trained over D , E and B to minimize the loss. Theorem 1 ensures worst-case guarantees for this two phase training (see the third remark afterwards). Figure 8 reports the approximation error of an image from Imagenet. The red and green lines in Figure 8 correspond to the

⁴Close to zero entries are sampled uniformly at random according to a Gaussian distribution with mean zero and variance 0.01.

⁵PCA stands for principal component analysis which is a standard way to compute X_k .

Figure 6: Approximation error with various methods for various values of k on the following data matrices from left to right: Gaussian 1, Gaussian 2, and MNISTFigure 7: Approximation error with various methods for various values of k on the following data matrices from left to right: Olivetti and Hyper

approximation error at the end of phase one and two respectively. Compared to training the entire network (represented by the yellow line in Figure 8) as done in Section 5.2, two phase training enjoys a smaller final loss and a faster rate of convergence.

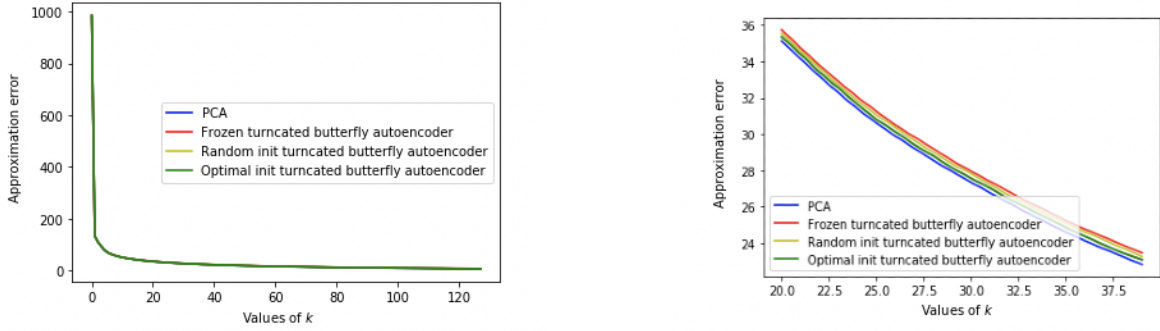
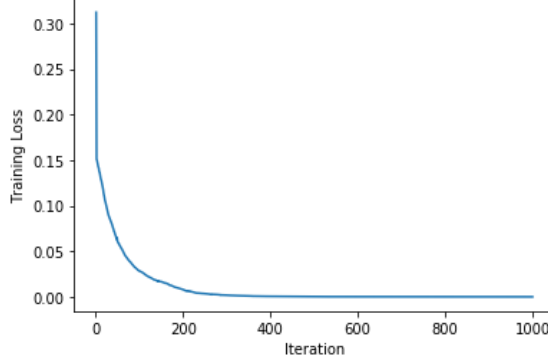


Figure 8: Approximation error achieved by different methods and the same zoomed on in the right

5.4 Learning Butterfly Weights for Data Generated by a Butterfly Network

Let $X \in \mathbb{R}^{n \times n}$ be a Gaussian matrix, $B \in \mathbb{R}^{k \times n}$ be a matrix constructed by choosing the entries of the $k \times n$ truncated butterfly gadget uniformly at random from the Gaussian distribution, and let $Y = BX$. This experiment learns the weights in the $k \times n$ truncated butterfly gadget B such that for $\bar{Y} = BX$, $\|\bar{Y} - Y\|_F^2$ is minimized. The network is optimized using the Adam optimizer. In Figure 9, it is seen that the error is zero after about thousand iterations indicating gradient descent methods learn the truncated butterfly representations exactly.

Figure 9: Training Loss of truncated butterfly network per iteration ($n = 1024, k = 10$)

5.5 Sketching Algorithm for Low-Rank Matrix Decomposition Problem Using Butterfly Networks

This experiment was inspired by the recent influential work by Indyk et al. [IVY19], which considers a supervised learning approach to compute an $\ell \times n$ pre-conditioning matrix B , where $\ell \ll n$, such that for $X \in \mathbb{R}^{n \times d}$, the best rank k approximation of X from the rows of BX (denoted $B_k(X)$) is optimized. The matrix B has a fixed sparse structure determined a priori as in [CW09], and the non-zero entries are learned to minimize the loss over a training set of matrices. The results in [IVY19] suggest that a learned matrix B significantly improves the guarantee compared to a random sketching matrix as in [CW09]. Our setting is similar to that in [IVY19], except that B is now represented as an $\ell \times n$ truncated butterfly gadget. Our experiments on several datasets show that indeed a learned truncated butterfly gadget does better than a random matrix, and even a learned B as in [IVY19].

Suppose $X_1, \dots, X_t \in \mathbb{R}^{n \times d}$ are training matrices sampled from a distribution \mathcal{D} . Then a B is computed that minimizes the following empirical loss

$$\sum_{i \in [t]} \|X_i - B_k(X_i)\|_F^2 \quad (2)$$

We compute $B_k(X_i)$ using truncated SVD of BX_i (as in Algorithm 1, [IVY19]). Similar to [IVY19], the matrix B is learned by the back-propagation algorithm that uses a differentiable SVD implementation to calculate the gradients, followed by optimization with Adam such that the butterfly structure of B is maintained. The learned B can be used as the pre-processing matrix for any matrix in the future.

The test error for a matrix B and a test set Te is defined as follows:

$$\text{Err}_{\text{Te}}(B) = \mathbb{E}_{X \sim \text{Te}} [\|X - B_k(X)\|_F^2] - \text{App}_{\text{Te}}, \quad \text{where } \text{App}_{\text{Te}} = \mathbb{E}_{X \sim \text{Te}} [\|X - X_k\|_F^2].$$

The experiments are performed on the datasets shown in Table 3. In HS-SOD [IOZ⁺18] and CIFAR-10 [Kri09] 400 training matrices ($t = 400$), and 100 test matrices are sampled, while in Tech 200 training matrices ($t = 200$), and 95 test matrices are sampled. In Tech [DGM04] each matrix has 835,422 rows but on average only 25,389 rows and 195 columns contain non-zero entries. For the same reason as in Section 5.2 in each dataset, the coordinates of each row are randomly permuted. Some of the matrices in the datasets have much larger singular values than the others, and to avoid imbalance in the dataset, the matrices are normalized so that their top singular values are all equal, as done in [IVY19]. For each of the datasets, the test error for the learned B via our truncated butterfly structure is compared

Name	n	d
HS-SOD 1	1024	768
CIFAR-10	32	32
Tech	25,389	195

Table 3: Data used in the Sketching algorithm for low-rank matrix decomposition experiments.

to the test errors for the following three cases: 1) B is learned as a sparse sketching matrix as in [IVY19], b) B is a random sketching matrix as in [CW09], and c) B is an $\ell \times n$ Gaussian matrix. Figure 10 compares the test error for $\ell = 20$, and $k = 10$, where $\text{App}_{\text{Te}} = 10.56$. Figure 13 in Appendix A compares the test errors of the different methods in the extreme case when $k = 1$, and Figure 14 in Appendix A compares the test errors of the different methods for

various values of ℓ . Table 4 in Appendix A reports the test error for different values of ℓ and k . Figure 11 shows the test error for $\ell = 20$ and $k = 10$ during the training phase on HS-SOD. Observe that the butterfly learned is able to surpass sparse learned after a merely few iterations.

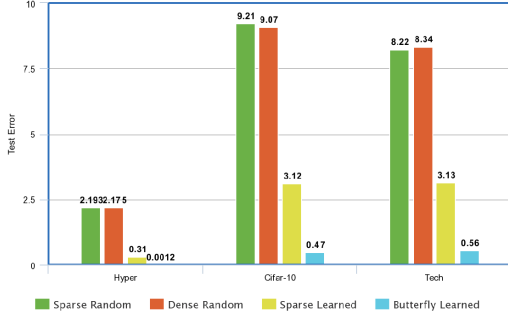


Figure 10: Test error by different sketching matrices on different data sets

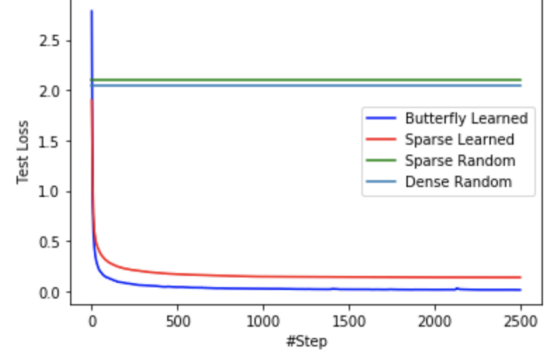


Figure 11: Test error when $k = 10$, $\ell = 20$ during the training phase on HS-SOD

Figure 12 compares the test error for the learned B via our truncated butterfly structure to a learned B with N non-zero entries in each column – the N non-zero locations of each column are chosen uniformly at random. The reported test errors are on HS-SOD, when $\ell = 20$ and $k = 10$. Note that $N = 1$ is the same as the sparse sketching matrix as in [IVY19], and $N = 20$ represents a dense learned matrix. Interestingly, the error for butterfly learned is not only less than the errors for sparse learned but also less than the error for dense learned. In particular, our results indicate that using a learned butterfly sketch can significantly reduce the approximation loss compared to using a learned sparse sketching matrix.

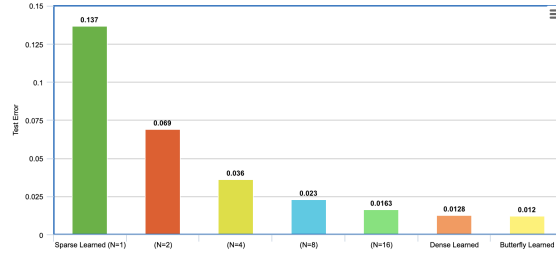


Figure 12: Test errors for various values of N and a learned butterfly matrix

6 Theoretical Results

In this section, the optimization landscape of the encoder-decoder network with a butterfly gadget (see Section 4.2) is studied. Before proceeding, we introduce a few notations. The loss \mathcal{L} is a function from the parameter space to reals. For an instance $\bar{Y} = DEBX$ of the network, the loss at D, E, B is $\mathcal{L}(\bar{Y}) \stackrel{\text{def}}{=} \|\bar{Y} - Y\|_F^2$. Theorem 1 shows that the loss at a critical point depends on the eigenvalues of $\Sigma(B) = YX^TB^T(BXX^TB^T)^{-1}XY^T$, when BXX^TB^T is invertible and $\Sigma(B)$ has ℓ distinct positive eigenvalues.

Theorem 1. *Let D, E and B be a point of the encoder-decoder network with a truncated butterfly network satisfying the following: a) BXX^TB^T is invertible, b) $\Sigma(B)$ has ℓ distinct positive eigenvalues $\lambda_1 > \dots > \lambda_\ell$, and c) the gradient of $\mathcal{L}(\bar{Y})$ with respect to the parameters in D and E matrix is zero. Then corresponding to this point (and hence corresponding to every critical point) there is an $I \subseteq [\ell]$ such that $\mathcal{L}(\bar{Y})$ at this point is equal to $\text{tr}(YY^T) - \sum_{i \in I} \lambda_i$. Moreover if the point is a local minima then $I = [k]$.*

The proof of Theorem 1 follows from techniques in [BH89] and is given in Appendix B. Following are a few remarks and conclusions drawn from Theorem 1.

1. *Comparison with [BH89, Kaw16]:* The critical points of the encoder-decoder network are analyzed in [BH89]. Suppose the eigenvalues of $YX^T(XX^T)^{-1}XY^T$ are $\gamma_1 > \dots > \gamma_m > 0$ and $k \leq m \leq n$. Then they show that corresponding to a critical point there is an $I \subseteq [m]$ such that the loss at this critical point is equal to

$\text{tr}(YY^T) - \sum_{i \in I} \gamma_i$, and the critical point is a local/global minima if and only if $I = [k]$. [Kaw16] later generalized this to prove that a local minima is a global minima for an arbitrary number of hidden layers in a linear neural network if $m \leq n$. Note that since $\ell \leq n$ and $m \leq n$ in Theorem 1, replacing X by BX in [BH89] or [Kaw16] does not imply Theorem 1 as it is.

2. *Fixed butterfly gadget*: If B is fixed and only D and E are trained then a local minima is indeed a global minima. Moreover, the butterfly gadget B in the theorem can be replaced by any structured matrix. For example the result continues to hold if B is an $\ell \times n$ matrix with one non-zero entry per column, as is the case with a random sparse sketching matrix [CW09].
3. *Two phase learning for auto-encoder*: Let $\ell = k \log k + k/\epsilon$ and consider a two phase learning strategy for auto-encoders, as follows: In phase one B is sampled from an FJLT distribution, and then only D and E are trained keeping B fixed. Suppose the algorithm learns D' and E' at the end of phase one, and $X' = D'E'B$. Then Theorem 1 guarantees that, assuming $\Sigma(B)$ has ℓ distinct positive eigenvalues and D', E' are a local minima, $D' = D_B$, $E' = E_B$, and $X' = B_k(X)$. Namely X' is the best rank k approximation of X from the rows of BX . From [Sar06] with probability at least $\frac{1}{2}$, $\mathcal{L}(X') \leq (1 + \epsilon)\Delta_k$. In the second phase all three matrices are trained to improve the loss.

7 Discussion and Future Work

Among other things, this work showed that it is beneficial to replace dense linear layer in deep learning architectures with a more compact architecture (in terms of number of parameters), using truncated butterfly gadgets. This approach is justified using ideas from efficient matrix approximation theory from the last two decades. The butterfly gadget, however, results in additional logarithmic depth to the network. This issue raises the question of whether the extra depth may harm convergence of gradient descent optimization. To start answering this question, we show, both empirically and theoretically, that in linear encoder-decoder networks in which the encoding is done using a butterfly gadget, this typically does not happen.

We also consider a supervised learning approach as in [IVY19], where we learn how to derive low rank approximations of a distribution of matrices by multiplying a pre-processing linear operator represented as a butterfly gadget, with weights trained using a sample of the distribution.

The main open questions arising from the work are related to better understanding the optimization landscape of butterfly gadgets. The current tools for analysis of deep linear networks do not apply for these structures, and more theory is necessary. An interesting open question is whether replacing dense linear layers in any network, with butterfly gadgets as in Section 4.1, *does not harm* convergence of the original matrix? How do we tune the structure parameters of these gadgets in order to ensure this?

Acknowledgement

This project has received funding from European Union’s Horizon 2020 research and innovation program under grant agreement No 682203 -ERC-[Inf-Speed-Tradeoff].

References

- [ABV18] Alan Akbik, Duncan Blythe, and Roland Vollgraf. Contextual string embeddings for sequence labeling. In *COLING 2018, 27th International Conference on Computational Linguistics*, pages 1638–1649, 2018.
- [ABV19] Alan Akbik, Tanja Bergmann, and Roland Vollgraf. Pooled contextualized embeddings for named entity recognition. In *NAACL 2019, 2019 Annual Conference of the North American Chapter of the Association for Computational Linguistics*, page 724–728, 2019.
- [AC09] Nir Ailon and Bernard Chazelle. The fast johnson–lindenstrauss transform and approximate nearest neighbors. *SIAM J. Comput.*, 39(1):302–322, 2009.
- [AL09] Nir Ailon and Edo Liberty. Fast dimension reduction using rademacher series on dual BCH codes. *Discret. Comput. Geom.*, 42(4):615–630, 2009.
- [AM10] Haim Avron and Petar Maymounkov. Blendenpik: Supercharging lapack’s least-squares solver. *SIAM J. Scientific Computing*, 32:1217–1236, 01 2010.
- [BH89] Pierre Baldi and Kurt Hornik. Neural networks and principal component analysis: Learning from examples without local minima. *Neural Networks*, 2(1):53–58, 1989.

- [Cad18] Remi Cadene. <https://github.com/Cadene/pretrained-models.pytorch>, 2018.
- [Cam94] AT&T Laboratories Cambridge. The olivetti faces dataset. 1992-1994.
- [CDY09] Emmanuel J. Candès, Laurent Demanet, and Lexing Ying. A fast butterfly algorithm for the computation of fourier integral operators. *Multiscale Model. Simul.*, 7(4):1727–1750, 2009.
- [CT65] J.W. Cooley and J.W. Tukey. An algorithm for the machine calculation of complex fourier series. *Mathematics of Computation*, 19(90):297–301, 1965.
- [CW09] Kenneth L. Clarkson and David P. Woodruff. Numerical linear algebra in the streaming model. In Michael Mitzenmacher, editor, *Proceedings of the 41st Annual ACM Symposium on Theory of Computing, STOC 2009*, pages 205–214. ACM, 2009.
- [CYF⁺15] Yu Cheng, Felix X. Yu, Rogério Schmidt Feris, Sanjiv Kumar, Alok N. Choudhary, and Shih-Fu Chang. An exploration of parameter redundancy in deep networks with circulant projections. In *2015 IEEE International Conference on Computer Vision, ICCV 2015, Santiago, Chile, December 7-13, 2015*, pages 2857–2865. IEEE Computer Society, 2015.
- [DDS⁺09] J. Deng, W. Dong, R. Socher, L.-J. Li, K. Li, and L. Fei-Fei. ImageNet: A Large-Scale Hierarchical Image Database. In *CVPR09*, 2009.
- [DGE⁺19] Tri Dao, Albert Gu, Matthew Eichhorn, Atri Rudra, and Christopher Ré. Learning fast algorithms for linear transforms using butterfly factorizations. In Kamalika Chaudhuri and Ruslan Salakhutdinov, editors, *Proceedings of the 36th International Conference on Machine Learning, ICML 2019, 9-15 June 2019, Long Beach, California, USA*, volume 97 of *Proceedings of Machine Learning Research*, pages 1517–1527. PMLR, 2019.
- [DGM04] D. Davido, E. Gabrilovich, and S. Markovitch. Parameterized generation of labeled datasets for text categorization based on a hierarchical directory. In *27th Annual International ACM SIGIR Conference on Research and Development in Information Retrieval, SIGIR '04*, pages 250–257, 2004.
- [DLW⁺17] Caiwen Ding, Siyu Liao, Yanzhi Wang, Zhe Li, Ning Liu, Youwei Zhuo, Chao Wang, Xuehai Qian, Yu Bai, Geng Yuan, Xiaolong Ma, Yipeng Zhang, Jian Tang, Qinru Qiu, Xue Lin, and Bo Yuan. Circnn: accelerating and compressing deep neural networks using block-circulant weight matrices. In *Proceedings of the 50th Annual IEEE/ACM International Symposium on Microarchitecture, MICRO 2017*, pages 395–408. ACM, 2017.
- [DSD⁺13] Misha Denil, Babak Shakibi, Laurent Dinh, Marc’Aurelio Ranzato, and Nando de Freitas. Predicting parameters in deep learning. In *Advances in Neural Information Processing Systems 26: 27th Annual Conference on Neural Information Processing Systems 2013.*, pages 2148–2156, 2013.
- [DY12] Laurent Demanet and Lexing Ying. Fast wave computation via fourier integral operators. *Math. Comput.*, 81(279):1455–1486, 2012.
- [IOZ⁺18] N. Imamoglu, Y. Oishi, X. Zhang, Y. Fang G. Ding, T. Kouyama, and R. Nakamura. Hyperspectral image dataset for benchmarking on salient object detection. In *Tenth International Conference on Quality of Multimedia Experience, (QoMEX)*, pages 1–3, 2018.
- [IVY19] Piotr Indyk, Ali Vakilian, and Yang Yuan. Learning-based low-rank approximations. In Hanna M. Wallach, Hugo Larochelle, Alina Beygelzimer, Florence d’Alché-Buc, Emily B. Fox, and Roman Garnett, editors, *Advances in Neural Information Processing Systems 32: Annual Conference on Neural Information Processing Systems 2019, NeurIPS 2019*, pages 7400–7410, 2019.
- [JL84] William Johnson and Joram Lindenstrauss. Extensions of lipschitz maps into a hilbert space. *Contemporary Mathematics*, 26:189–206, 01 1984.
- [JPS20] Vishesh Jain, Natesh Pillai, and Aaron Smith. Kac meets johnson and lindenstrauss: a memory-optimal, fast johnson-lindenstrauss transform. *arXiv*, 03 2020.
- [Kaw16] Kenji Kawaguchi. Deep learning without poor local minima. In *Advances in Neural Information Processing Systems 29: Annual Conference on Neural Information Processing Systems 2016, December 5-10, 2016, Barcelona, Spain*, pages 586–594, 2016.
- [Kri09] Alex Krizhevsky. Learning multiple layers of features from tiny images. Technical report, 2009.
- [Kua] Kuangliu. <https://github.com/kuangliu/pytorch-cifar>.
- [KW11] Felix Krahmer and Rachel Ward. New and improved johnson–lindenstrauss embeddings via the restricted isometry property. *SIAM Journal on Mathematical Analysis*, 43:1269–1281, 06 2011.
- [LC10] Yann LeCun and Corinna Cortes. MNIST handwritten digit database. 2010.

- [LSS16] Zhiyun Lu, Vikas Sindhwani, and Tara N. Sainath. Learning compact recurrent neural networks. In *2016 IEEE International Conference on Acoustics, Speech and Signal Processing, ICASSP 2016*, pages 5960–5964. IEEE, 2016.
- [LY17] Yingzhou Li and Haizhao Yang. Interpolative butterfly factorization. *SIAM J. Scientific Computing*, 39(2), 2017.
- [LYM⁺15] Yingzhou Li, Haizhao Yang, Eileen R. Martin, Kenneth L. Ho, and Lexing Ying. Butterfly factorization. *Multiscale Model. Simul.*, 13(2):714–732, 2015.
- [LYY15] Yingzhou Li, Haizhao Yang, and Lexing Ying. A multiscale butterfly algorithm for multidimensional fourier integral operators. *Multiscale Model. Simul.*, 13(2):614–631, 2015.
- [MB96] E. Michielssen and A. Boag. A multilevel matrix decomposition algorithm for analyzing scattering from large structures. *IEEE Transactions on Antennas and Propagation*, 44(8):1086–1093, 1996.
- [MDAdF16] Marcin Moczulski, Misha Denil, Jeremy Appleyard, and Nando de Freitas. ACDC: A structured efficient linear layer. In Yoshua Bengio and Yann LeCun, editors, *4th International Conference on Learning Representations, ICLR 2016*, 2016.
- [MSM93] Mitchell P. Marcus, Beatrice Santorini, and Mary Ann Marcinkiewicz. Building a large annotated corpus of English: The Penn Treebank. *Computational Linguistics*, 19(2):313–330, 1993.
- [OWR10] Michael O’Neil, Franco Woolfe, and Vladimir Rokhlin. An algorithm for the rapid evaluation of special function transforms. *Applied and Computational Harmonic Analysis*, 28(2):203 – 226, 2010.
- [PDMY14] Jack Poulson, Laurent Demanet, Nicholas Maxwell, and Lexing Ying. A parallel butterfly algorithm. *SIAM J. Scientific Computing*, 36(1), 2014.
- [Sar06] Tamás Sarlós. Improved approximation algorithms for large matrices via random projections. In *47th Annual IEEE Symposium on Foundations of Computer Science (FOCS 2006)*, pages 143–152. IEEE Computer Society, 2006.
- [Sel12] D. S. Seljebotn. WAVEMOTH-FAST SPHERICAL HARMONIC TRANSFORMS BY BUTTERFLY MATRIX COMPRESSION. *The Astrophysical Journal Supplement Series*, 199(1):5, 2012.
- [SKS⁺13] Tara N. Sainath, Brian Kingsbury, Vikas Sindhwani, Ebru Arisoy, and Bhuvana Ramabhadran. Low-rank matrix factorization for deep neural network training with high-dimensional output targets. In *IEEE International Conference on Acoustics, Speech and Signal Processing, ICASSP 2013, Vancouver, BC, Canada, May 26-31, 2013*, pages 6655–6659. IEEE, 2013.
- [SSK15] Vikas Sindhwani, Tara N. Sainath, and Sanjiv Kumar. Structured transforms for small-footprint deep learning. In Corinna Cortes, Neil D. Lawrence, Daniel D. Lee, Masashi Sugiyama, and Roman Garnett, editors, *Advances in Neural Information Processing Systems 28: Annual Conference on Neural Information Processing Systems 2015*, pages 3088–3096, 2015.
- [TGD⁺18] Anna T. Thomas, Albert Gu, Tri Dao, Atri Rudra, and Christopher Ré. Learning compressed transforms with low displacement rank. In *Advances in Neural Information Processing Systems 31: Annual Conference on Neural Information Processing Systems 2018*, pages 9066–9078, 2018.
- [TKSDM03] Erik F. Tjong Kim Sang and Fien De Meulder. Introduction to the CoNLL-2003 shared task: Language-independent named entity recognition. In *Proceedings of the Seventh Conference on Natural Language Learning at HLT-NAACL 2003*, pages 142–147, 2003.
- [Wei] Weiaicunzai. <https://github.com/weiaicunzai/pytorch-cifar100>.
- [Yin09] Lexing Ying. Sparse fourier transform via butterfly algorithm. *SIAM J. Scientific Computing*, 31(3):1678–1694, 2009.
- [YMD⁺15] Zichao Yang, Marcin Moczulski, Misha Denil, Nando de Freitas, Alexander J. Smola, Le Song, and Ziyu Wang. Deep fried convnets. In *2015 IEEE International Conference on Computer Vision, ICCV 2015*, pages 1476–1483. IEEE Computer Society, 2015.
- [YWL⁺18] Jinmian Ye, Linnan Wang, Guangxi Li, Di Chen, Shandian Zhe, Xinqi Chu, and Zenglin Xu. Learning compact recurrent neural networks with block-term tensor decomposition. In *2018 IEEE Conference on Computer Vision and Pattern Recognition, CVPR 2018*, pages 9378–9387. IEEE Computer Society, 2018.

A Additional Plots from Section 5.5

Figure 13 compares the test errors of the different methods in the extreme case when $k = 1$. Figure 14 compares the test errors of the different methods for various values of ℓ . Finally Table 4 compares the test error for different values of ℓ and k .

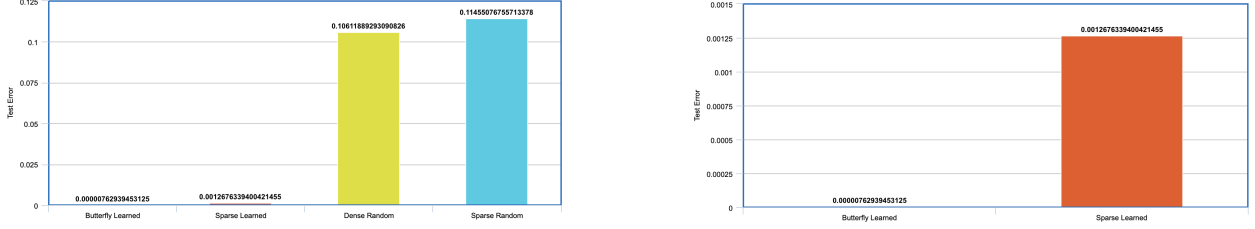


Figure 13: Test errors on HS-SOD for $\ell = 20$ and $k = 1$ and on the right the same is zoomed over butterfly learned and sparse learned

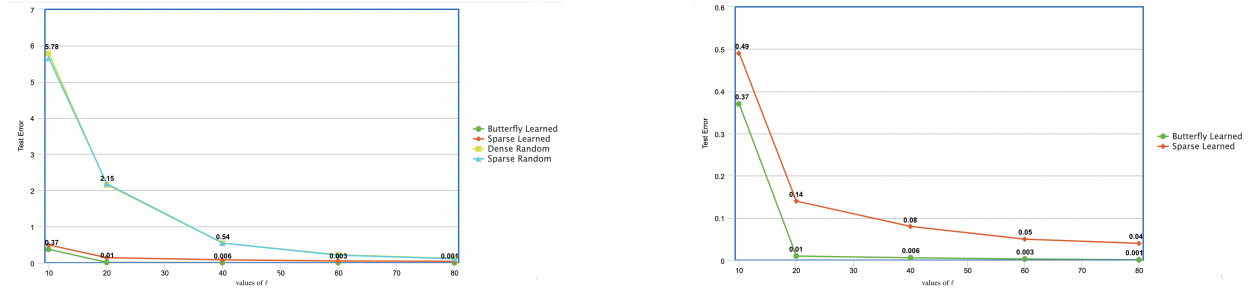


Figure 14: Test error when $k = 10$, $\ell = [10, 20, 40, 60, 80]$ on HS-SOD and on the right the same is zoomed over butterfly learned and sparse learned

B Proof of Theorem 1

We introduce a few notation before delving into the proof. Let $r = (\bar{Y} - Y)^T$, and $\text{vec}(r) \in \mathbb{R}^{md}$ is the entries of r arranged as a vector in column-first ordering, $(\nabla_{\text{vec}(D^T)} \mathcal{L}(\bar{Y}))^T \in \mathbb{R}^{mk}$ and $(\nabla_{\text{vec}(E^T)} \mathcal{L}(\bar{Y}))^T \in \mathbb{R}^{k\ell}$ denote the partial derivative of $\mathcal{L}(\bar{Y})$ with respect to the parameters in $\text{vec}(D^T)$ and $\text{vec}(E^T)$ respectively. Notice that $\nabla_{\text{vec}(D^T)} \mathcal{L}(\bar{Y})$ and $\nabla_{\text{vec}(E^T)} \mathcal{L}(\bar{Y})$ are row vectors of size mk and $k\ell$ respectively. Also, let P_D denote the projection matrix of D , and hence if D is a matrix with full column-rank then $P_D = D(D^T D)^{-1} D^T$. The $n \times n$ identity matrix is denoted as I_n , and for ease of notation let $\tilde{X} = BX$. First we prove the following lemma which is used later to derive an expression for D and E if $\nabla_{\text{vec}(D^T)} \mathcal{L}(\bar{Y})$ and $\nabla_{\text{vec}(E^T)} \mathcal{L}(\bar{Y})$ are zero. In Lemma B.1 we use the fact that $\nabla_{\text{vec}(D^T)} \text{vec}(D^T) = I_{mk}$, and $\nabla_{\text{vec}(E^T)} \text{vec}(E^T) = I_{k\ell}$.

Lemma B.1 (Derivatives with respect to D and E).

1. $\nabla_{\text{vec}(D^T)} \mathcal{L}(\bar{Y}) = \text{vec}(r)^T (I_m \otimes (E \tilde{X})^T)$, and
2. $\nabla_{\text{vec}(E^T)} \mathcal{L}(\bar{Y}) = \text{vec}(r)^T (D \otimes \tilde{X})^T$

Proof. 1. Since $\mathcal{L}(\bar{Y}) = \frac{1}{2} \text{vec}(r)^T \text{vec}(r)$,

$$\begin{aligned} \nabla_{\text{vec}(D^T)} \mathcal{L}(\bar{Y}) &= \text{vec}(r)^T \cdot \nabla_{\text{vec}(D^T)} \text{vec}(r) = \text{vec}(r)^T \cdot \nabla_{\text{vec}(D^T)} (\text{vec}(\tilde{X}^T E^T D^T)) \\ &= \text{vec}(r)^T (I_m \otimes (E \tilde{X})^T) \cdot \nabla_{\text{vec}(D^T)} \text{vec}(D^T) = \text{vec}(r)^T (I_m \otimes (E \tilde{X})^T) \end{aligned}$$

2. Similarly,

$$\begin{aligned} \nabla_{\text{vec}(E^T)} \mathcal{L}(\bar{Y}) &= \text{vec}(r)^T \cdot \nabla_{\text{vec}(E^T)} \text{vec}(r) = \text{vec}(r)^T \cdot \nabla_{\text{vec}(E^T)} (\text{vec}(\tilde{X}^T E^T D^T)) \\ &= \text{vec}(r)^T (D \otimes \tilde{X})^T \cdot \nabla_{\text{vec}(E^T)} \text{vec}(E^T) = \text{vec}(r)^T (D \otimes \tilde{X})^T \end{aligned}$$

□

k, ℓ, Sketch	Hyper	Cifar-10	Tech
1, 5, Butterfly	0.0008	0.173	0.188
1, 5, Sparse	0.003	1.121	1.75
1, 5, Random	0.661	4.870	3.127
1, 10, Butterfly	0.0002	0.072	0.051
1, 10, Sparse	0.002	0.671	0.455
1, 10, Random	0.131	1.82	1.44
10, 10, Butterfly	0.031	0.751	0.619
10, 10, Sparse	0.489	6.989	7.154
10, 10, Random	5.712	26.133	18.805
10, 20, Butterfly	0.012	0.470	0.568
10, 20, Sparse	0.139	3.122	3.134
10, 20, Random	2.097	9.216	8.22
10, 40, Butterfly	0.006		0.111
10, 40, Sparse	0.081		0.991
10, 40, Random	0.544		3.304
20, 20, Butterfly	0.058		1.38
20, 20, Sparse	0.229		8.14
20, 20, Random	4.173		15.268
20, 40, Butterfly	0.024		0.703
20, 40, Sparse	0.247		3.441
20, 40, Random	1.334		6.848
30, 30, Butterfly	0.027		1.25
30, 30, Sparse	0.749		7.519
30, 30, Random	3.486		13.168
30, 60, Butterfly	0.014		0.409
30, 60, Sparse	0.331		2.993
30, 60, Random	2.105		5.124

Table 4: Test error for different ℓ and k

Assume the rank of D is equal to p . Hence there is an invertible matrix $C \in \mathbb{R}^{k \times k}$ such that the last $k - p$ columns of $\tilde{D} = DC$ are zero and its first p columns is linearly independent (via Gauss elimination). Let $\tilde{E} = C^{-1}E$. Without loss of generality it can be assumed $\tilde{D} \in \mathbb{R}^{d \times p}$, and $\tilde{E} \in \mathbb{R}^{p \times d}$, by restricting \tilde{D} to its first p columns (as the remaining are zero) and \tilde{E} to its first p rows. Hence, \tilde{D} is a full column-rank matrix of rank p , and $DE = \tilde{D}\tilde{E}$. Claims B.1 and B.2 aid us in the completing the proof of the theorem. First the proof of theorem is completed using these claims, and at the end the two claims are proved.

Claim B.1 (Representation at the critical point).

1. $\tilde{E} = (\tilde{D}^T \tilde{D})^{-1} \tilde{D}^T Y \tilde{X}^T (\tilde{X} \cdot \tilde{X}^T)^{-1}$
2. $\tilde{D} \tilde{E} = P_{\tilde{D}} Y \tilde{X}^T (\tilde{X} \cdot \tilde{X}^T)^{-1}$

Claim B.2. 1. $\tilde{E} B \tilde{D} = (\tilde{E} B Y \tilde{X}^T \tilde{E}^T) (\tilde{E} \tilde{X} \tilde{X}^T \tilde{E}^T)^{-1}$

2. $P_{\tilde{D}} \Sigma = \Sigma P_{\tilde{D}} = P_{\tilde{D}} \Sigma P_{\tilde{D}}$

We denote $\Sigma(B)$ as Σ for convenience. Since Σ is a real symmetric matrix, there is an orthogonal matrix U consisting of the eigenvectors of Σ , such that $\Sigma = U \Lambda U^T$, where Λ is a $m \times m$ diagonal matrix whose first ℓ diagonal entries are $\lambda_1, \dots, \lambda_\ell$ and the remaining entries are zero. Let u_1, \dots, u_m be the columns of U . Then for $i \in [\ell]$, u_i is the eigenvector of Σ corresponding to the eigenvalue λ_i , and $\{u_{\ell+1}, \dots, u_d\}$ are the eigenvectors of Σ corresponding to the eigenvalue 0.

Note that $P_{U^T \tilde{D}} = U^T \tilde{D} (\tilde{D}^T U^T U \tilde{D})^{-1} \tilde{D}^T U = U^T P_{\tilde{D}} U$, and from part two of Claim B.2 we have

$$(U P_{U^T \tilde{D}} U^T) \Sigma = \Sigma (U P_{U^T \tilde{D}} U^T) \quad (3)$$

$$U \cdot P_{U^T \tilde{D}} \wedge U^T = U \wedge P_{U^T \tilde{D}} U^T \quad (4)$$

$$P_{U^T \tilde{D}} \wedge = \wedge P_{U^T \tilde{D}} \quad (5)$$

Since $P_{U^T \tilde{D}}$ commutes with \wedge , $P_{U^T \tilde{D}}$ is a block-diagonal matrix comprising of two blocks P_1 and P_2 : the first block P_1 is an $\ell \times \ell$ diagonal block, and P_2 is a $(m - \ell) \times (m - \ell)$ matrix. Since $P_{U^T \tilde{D}}$ is orthogonal projection matrix of rank p its eigenvalues are 1 with multiplicity p and 0 with multiplicity $m - p$. Hence at most p diagonal entries of P_1 are 1 and the remaining are 0. Finally observe that

$$\begin{aligned} \mathcal{L}(\bar{Y}) &= \text{tr}((\bar{Y} - Y)(\bar{Y} - Y)^T) \\ &= \text{tr}(YY^T) - 2\text{tr}(\bar{Y}Y^T) + \text{tr}(\bar{Y}\bar{Y}^T) \\ &= \text{tr}(YY^T) - 2\text{tr}(P_{\tilde{D}}\Sigma) + \text{tr}(P_{\tilde{D}}\Sigma P_{\tilde{D}}) \\ &= \text{tr}(YY^T) - \text{tr}(P_{\tilde{D}}\Sigma) \end{aligned}$$

The second line in the above equation follows using the fact that $\text{tr}(\bar{Y}Y^T) = \text{tr}(Y\bar{Y}^T)$, the third line in the above equation follows by substituting $\bar{Y} = P_{\tilde{D}}Y\tilde{X}^T \cdot (\tilde{X} \cdot \tilde{X}^T)^{-1} \cdot \tilde{X}$ (from part two of Claim B.1), and the last line follows from part two of Claim B.2. Substituting $\Sigma = U \wedge U^T$, and $P_{\tilde{D}} = UP_{U^T \tilde{D}}U^T$ in the above equation we have,

$$\begin{aligned} \mathcal{L}(\bar{Y}) &= \text{tr}(YY^T) - \text{tr}(UP_{U^T \tilde{D}} \wedge U^T) \\ &= \text{tr}(YY^T) - \text{tr}(P_{U^T \tilde{D}} \wedge) \end{aligned}$$

The last line the above equation follows from the fact that $\text{tr}(UP_{U^T \tilde{D}} \wedge U^T) = \text{tr}(P_{U^T \tilde{D}} \wedge U^T U) = \text{tr}(P_{U^T \tilde{D}} \wedge)$. From the structure of $P_{U^T \tilde{D}}$ and \wedge it follows that there is a subset $I \subseteq [\ell]$, $|I| \leq p$ such that $\text{tr}(P_{U^T \tilde{D}} \wedge) = \sum_{i \in I} \lambda_i$. Hence, $\mathcal{L}(\bar{Y}) = \text{tr}(YY^T) - \sum_{i \in I} \lambda_i$.

Since $P_{\tilde{D}} = UP_{U^T \tilde{D}}U^T$, there is a $p \times p$ invertible matrix M such that

$$\tilde{D} = (U \cdot V)_{I'} \cdot M, \text{ and } \tilde{E} = M^{-1}(V^T U^T)_{I'} Y \tilde{X}^T (\tilde{X} \tilde{X}^T)^{-1}$$

where V is a block-diagonal matrix consisting of two blocks V_1 and V_2 : V_1 is equal to I_ℓ , and V_2 is an $(m - \ell) \times (m - \ell)$ orthogonal matrix, and I' is such that $I \subseteq I'$ and $|I'| = p$. The relation for \tilde{E} in the above equation follows from part one of Claim B.1. Note that if $I' \subseteq [\ell]$, then $I = I'$, that is I consists of indices corresponding to eigenvectors of non-zero eigenvalues.

Recall that \tilde{D} was obtained by truncating the last $k - p$ zero rows of DC , where C was a $k \times k$ invertible matrix simulating the Gaussian elimination. Let $[M|O_{p \times (k-p)}]$ denoted the $p \times k$ matrix obtained by augmenting the columns of M with $(k - p)$ zero columns. Then

$$D = (UV)_{I'} [M|O_{p \times (k-p)}] C^{-1}.$$

Similarly, there is a $p \times (k - p)$ matrix N such that

$$E = C[\frac{M^{-1}}{N}]((UV)_{I'})^T Y \tilde{X}^T (\tilde{X} \tilde{X}^T)^{-1}$$

where $[\frac{M^{-1}}{N}]$ denotes the $k \times p$ matrix obtained by augmenting the rows of M^{-1} with the rows of N . Now suppose $I \neq [k]$, and hence $I' \neq [k]$. Then we will show that there are matrices D' and E' arbitrarily close to D and E respectively such that if $Y' = D'E'\tilde{X}$ then $\mathcal{L}(Y') < \mathcal{L}(\bar{Y})$. There is an $a \in [k] \setminus I'$, and $b \in I'$ such that $\lambda_a > \lambda_b$ (λ_b could also be zero). Denote the columns of the matrix UV as $\{v_1, \dots, v_m\}$, and observe that $v_i = u_i$ for $i \in [\ell]$ (from the structure of V). For $\epsilon > 0$ let $u'_b = (1 + \epsilon^2)^{-\frac{1}{2}}(v_b + \epsilon u_a)$. Define U' as the matrix which is equal to UV except that the column vector v_b in UV is replaced by u'_b in U' . Since $a \in [k] \subseteq [\ell]$ and $a \notin I'$, $v_a = u_a$ and $(U'_{I'})^T U'_{I'} = I_p$. Define

$$D' = U'_{I'} [M|O_{p \times (k-p)}] C^{-1}, \text{ and } E' = C[\frac{M^{-1}}{N}](U'_{I'})^T Y \tilde{X}^T (\tilde{X} \tilde{X}^T)^{-1}$$

and let $Y' = D'E'\tilde{X}$. Now observe that, $D'E' = U'_{I'}(U'_{I'})^T Y \tilde{X}^T (\tilde{X} \tilde{X}^T)^{-1}$, and that

$$\mathcal{L}(Y') = \text{tr}(YY^T) - \sum_{i \in I} \lambda_i - \frac{\epsilon^2}{1 + \epsilon^2}(\lambda_a - \lambda_b) = \mathcal{L}(\bar{Y}) - \frac{\epsilon^2}{1 + \epsilon^2}(\lambda_a - \lambda_b)$$

Since ϵ can be set arbitrarily close to zero, it can be concluded that there are points in the neighbourhood of \bar{Y} such that the loss at these points are less than $\mathcal{L}(\bar{Y})$. Further, since \mathcal{L} is convex with respect to the parameters in D (respectively E), when the matrix E is fixed (respectively D is fixed) \bar{Y} is not a local maximum. Hence, if $I \neq [k]$ then \bar{Y} represents a saddle point, and in particular \bar{Y} is local/global minima if and only if $I = [k]$.

Proof of Claim B.1. Since $\nabla_{\text{vec}(E^T)}\mathcal{L}(\bar{X})$ is equal to zero, from the second part of Lemma B.1 the following holds,

$$\begin{aligned} \tilde{X}(Y - \bar{Y})^T D &= \tilde{X}Y^T D - \tilde{X}\bar{Y}^T D = 0 \\ \Rightarrow \tilde{X}\tilde{X}^T E^T D^T D &= \tilde{X}Y^T D \end{aligned}$$

Taking transpose on both sides

$$\Rightarrow D^T D E \tilde{X} \tilde{X}^T = D^T Y \tilde{X}^T \quad (6)$$

Substituting DE as $\tilde{D}\tilde{E}$ in Equation 6, and multiplying Equation 6 by C^T on both the sides from the left, Equation 7 follows.

$$\Rightarrow \tilde{D}^T \tilde{D} \tilde{E} \tilde{X} \tilde{X}^T = \tilde{D}^T Y \tilde{X}^T \quad (7)$$

Since \tilde{D} is full-rank, we have

$$\tilde{E} = (\tilde{D}^T \tilde{D})^{-1} \tilde{D}^T Y \tilde{X}^T (\tilde{X} \tilde{X}^T)^{-1}. \quad (8)$$

and,

$$\tilde{D} \tilde{E} = P_{\tilde{D}} Y \tilde{X}^T (\tilde{X} \tilde{X}^T)^{-1} \quad (9)$$

□

Proof of Claim B.2. Since $\nabla_{\text{vec}(D^T)}\mathcal{L}(\bar{Y})$ is zero, from the first part of Lemma B.1 the following holds,

$$\begin{aligned} E \tilde{X}(Y - \bar{Y})^T &= E \tilde{X}Y^T - E \tilde{X}\bar{Y}^T = 0 \\ \Rightarrow E \tilde{X} \tilde{X}^T E^T D^T &= E \tilde{X}Y^T \end{aligned} \quad (10)$$

Substituting $E^T \cdot D^T$ as $\tilde{E}^T \cdot \tilde{D}^T$ in Equation 6, and multiplying Equation 10 by C^{-1} on both the sides from the left Equation 11 follows.

$$\tilde{E} \tilde{X} \tilde{X}^T \tilde{E}^T \tilde{D}^T = \tilde{E} \tilde{X}Y^T \quad (11)$$

Taking transpose of the above equation we have,

$$\tilde{D} \tilde{E} \tilde{X} \tilde{X}^T \tilde{E}^T = Y \tilde{X}^T \tilde{E}^T \quad (12)$$

From part 1 of Claim B.1, it follows that \tilde{E} has full row-rank, and hence $\tilde{E} \tilde{X} \tilde{X}^T \tilde{E}^T$ is invertible. Multiplying the inverse of $\tilde{E} \tilde{X} \tilde{X}^T \tilde{E}^T$ from the right on both sides and multiplying $\tilde{E}B$ from the left on both sides of the above equation we have,

$$\tilde{E}B\tilde{D} = (\tilde{E}B\tilde{X} \tilde{X}^T \tilde{E}^T)(\tilde{E} \tilde{X} \tilde{X}^T \tilde{E}^T)^{-1} \quad (13)$$

This proves part one of the claim. Moreover, multiplying Equation 12 by \tilde{D}^T from the right on both sides

$$\begin{aligned} \tilde{D} \tilde{E} \tilde{X} \tilde{X}^T \tilde{E}^T \tilde{D}^T &= Y \tilde{X}^T \tilde{E}^T \tilde{D}^T \\ \Rightarrow (P_{\tilde{D}} Y \tilde{X}^T (\tilde{X} \tilde{X}^T)^{-1}) (\tilde{X} \tilde{X}^T) ((\tilde{X} \tilde{X}^T)^{-1} \tilde{X} Y^T P_{\tilde{D}}) &= Y \tilde{X}^T ((\tilde{X} \tilde{X}^T)^{-1} \tilde{X} Y^T P_{\tilde{D}}) \\ \Rightarrow P_{\tilde{D}} Y \tilde{X}^T (\tilde{X} \tilde{X}^T)^{-1} \tilde{X} Y^T P_{\tilde{D}} &= Y \tilde{X}^T (\tilde{X} \tilde{X}^T)^{-1} \tilde{X} Y^T P_{\tilde{D}} \end{aligned}$$

The second line the above equation follows by substituting $\tilde{D} \tilde{E} = P_{\tilde{D}} Y \tilde{X}^T (\tilde{X} \tilde{X}^T)^{-1}$ (from part 2 of Claim B.1). Substituting $\Sigma = Y \tilde{X}^T (\tilde{X} \tilde{X}^T)^{-1} \tilde{X} Y^T$ in the above equation we have

$$P_{\tilde{D}} \Sigma P_{\tilde{D}} = \Sigma P_{\tilde{D}}$$

Since $P_{\tilde{D}}^T = P_{\tilde{D}}$, and $\Sigma^T = \Sigma$, we also have $\Sigma P_{\tilde{D}} = P_{\tilde{D}} \Sigma$. □